THE ASTRONOMICAL JOURNAL, 116:2475–2488, 1998 November

A NEW SYSTEM OF FAINT NEAR-INFRARED STANDARD STARS

S. E. PERSSON,[1] D. C. MURPHY,[1] W. KRZEMINSKI,[1] M. ROTH,[1] AND M. J. RIEKE[2]

Received 1998 June 3; revised 1998 July 28

ABSTRACT

A new grid of 65 faint near-infrared standard stars is presented. They are spread around the sky, lie between 10th and 12th magnitude at K, and are measured in most cases to precisions better than 0.001 mag in the J, H, K, and K_s bands; the latter is a medium-band modified K. A secondary list of red stars suitable for determining color transformations between photometric systems is also presented.

Key words: infrared radiation — stars: general — techniques: photometric

1. INTRODUCTION

Photometric measurements in the near-infrared were extended to faint limits and placed on a firm foundation with the work of Elias et al. (1982, henceforth E82), who presented accurate J, H, and K magnitudes for 40 stars near 7th magnitude at K. These new standard stars were measured with respect to a set of 4th magnitude standards, which had been established relative to α Lyrae. The uncertainties were generally smaller than 0.005 mag. Another paper which furthered the state of near-infrared standard star photometry was that of Campins, Rieke, & Lebofsky (1985). These authors advocated the use of solar-analog stars, and also established an accurate absolute calibration. Recent technological advances have created a need for a new set of yet fainter infrared standard stars. These include the advent of megapixel imaging arrays, telescopes significantly larger than were in use prior to 1982, the *Hubble Space Telescope* (*HST*) Near-Infrared Camera and Multiobject Spectrometer (NICMOS) camera system, and the recently commissioned 2MASS all-sky JHK-band survey. Essentially all imaging photometry in the near-infrared, i.e., in the 1 to 2.5 μm range, is now carried out with detector arrays, whose high quantum efficiencies and somewhat limited dynamic range motivated this program. We present J, H, K, and K_s magnitudes for 65 stars with $10 < K < 12$ spread around the sky. (The K_s filter is a modified K filter that reduces the thermal background for warm ground-based telescopes.) We also present data for 27 stars that span a range in $J-K$ color from 0 to 3, plus one with a $J-K$ color of 8. These stars can be used to transform between ours and other photometric color systems.

2. OBSERVATIONAL PROGRAM

2.1. *Sample Selection*

This program originated in 1993 as part of the image calibration plan for the NICMOS camera aboard *HST*. For the purposes of transforming *HST* NICMOS photometric data obtained with bandpasses different from those of conventional ground-based filter systems, we decided to devote most of the effort to stars with solar-type colors. Solar analogues have the minimum number of strong absorption features in the near-infrared of any spectral type and are also preferred for calibrating observations of solar system objects. Thus colors in the range $0.42 < (B-V) < 0.86$ and $E(B-V) < 0.16$ (as estimated from the Burstein & Heiles 1982 reddening maps) were chosen. Both the requirements of *HST* NICMOS and those of ground-based cameras on telescopes of apertures greater than 2.5 m indicated that K-band magnitudes around 11 would be best. A list of *HST* guide stars thus selected by color and magnitude from Lasker et al. (1988) was made, and various *HST* observability criteria were imposed. Additional stars were chosen to lie close in the sky to the best-measured E82 standards, in order to minimize air mass, time, and telescope pointing differences as the stars were being observed. The resulting list is concentrated along the equator, and at $\pm 40°$ declination. The red stars were selected from a literature search to span a wide range in $J-K$ color.

Two other sets of faint infrared standard stars are currently in use. Carter & Meadows (1995) published $JHKL$ magnitudes for stars in the range $K = 8$ to 9.5, and while the data appear to be accurate, the stars are rather bright to be practical for current array cameras on large telescopes. The UKIRT group (Casali & Hawarden 1992) has published data for a set of equatorial stars; comparisons with our data are given in § 5. Recently, a new set of northern standards based on the UKIRT system has appeared (Hunt et al. 1998); these are also discussed in § 5.

2.2. *Telescopes and Cameras*

Table 1 gives information on the telescopes and infrared cameras used in this program, and Tables 2 and 3 list the stars measured. In each case the detector was a NICMOS3 256 × 256 HgCdTe array produced by the Rockwell International Science Center (see, e.g., Vural 1994). The observations were carried out on the 1 m Swope Telescope at Las Campanas Observatory, Chile, and on the 60 inch (1.5 m) telescope at Palomar Observatory. The observational program was divided into three parts. In part 1, the IRCAM camera, normally mounted on the 2.5 m du Pont Telescope at Las Campanas, was used at two different imaging scales to establish directly the infrared magnitudes of 17 "new" standard stars with respect to the best-determined E82 standards, (viz., those of a or $a+$ quality). The 17 new standard stars observed in part 1 are noted with a 1 in the last column of Table 2. For the K_s magnitudes of the E82 standards we simply defined $K_s = K$.

A new infrared camera, the C40IRC, was placed into operation at Las Campanas in 1995 during part 1 of the program. It is quite similar to the Palomar infrared camera

[1] Observatories of the Carnegie Institution of Washington, 813 Santa Barbara Street, Pasadena, CA 91101.
[2] Steward Observatory, University of Arizona, 933 North Cherry Avenue, Tucson, AZ 85721.

TABLE 1

INFRARED CAMERAS AND OBSERVING RUNS

Part	Camera	Telescope	f-Ratio	Scale (arcsec pixel^{-1})	N (runs)	N (nights)	Camera Reference
1.....	IRCAM	LCO 1 m	7.0	0.43	14	44	1
1.....	IRCAM	LCO 1 m	13.5	0.22	2	7	1
2.....	C40IRC	LCO 1 m	13.5	0.60	16	75	2
3.....	P60IRC	Pal 1.5 m	8.75	0.62	7	13	3

REFERENCES.—(1) Persson et al. 1992; (2) this paper; (3) Murphy et al. 1995.

described by Murphy et al. (1995). Part 2 of the program consisted of using the C40IRC to extend the database from the southern and equatorial stars to an additional 30; for these observations the 17 stars from part 1 were treated as true standards. This procedure was necessitated by the fact that the new C40IRC camera produced sharper images and has higher throughput than the IRCAM, and that the relatively coarser pixel scale concentrated a larger fraction of the light into the central pixel(s). This meant that during periods of excellent seeing, and without defocusing or scanning the telescope, the E82 standards were too bright, i.e., the signal levels in the central pixel(s) were approaching the point where the adopted linearity correction was more than a few percent. These corrections are discussed below. A 2 (or 4) in the last column of Table 2 indicates southern (or equatorial) stars in this list.

Northern stars were observed on the Palomar 60 inch telescope with the P60IRC, a camera that was placed into operation in late 1994. The P60IRC is described by Murphy et al. (1995). Part 3 of the program consisted of using the equatorial standards of part 1 to extend the calibration into the northern sky, i.e., to declinations of approximately $+40°$. In addition, six equatorial stars measured in part 2 were repeated from Palomar as a consistency check. A 3 in the last column of Table 2 indicates those stars observed only from Palomar, while a 4 indicates that data were obtained using both telescopes.

2.3. *Observing Conditions and Procedures*

Observations on a typical night began with acquisition of twilight sky flat-field frames a few minutes after sunset. By the term "flat-field," we include only strictly multiplicative factors in the overall transmission of the telescope/camera combination. Regions of sky selected to be free of bright stars were used and the telescope was moved a few arcseconds between exposures. A scaled median of the (dark-subtracted) frames then produced a flat minimally affected by residual stars or by fringing, which is due mostly to bright atmospheric OH lines. During twilight these lines are much fainter than the continuum from the sky. Because our sources are essentially continuum objects, it is important to flatten the frames with flats that are also dominated by continuum emission. This procedure comes as close as is possible, in a practical sense, to ensuring that the frames are flattened in a purely multiplicative way. Flats were acquired at the beginning of every night, if possible, and were intercompared for consistency. These comparisons generally indicated that grand average twilight flats, one for each wavelength, for an entire observing run, would have the highest signal-to-noise ratios. A typical observation of a star consisted of acquiring a set of several frames at each of three to five positions on the array. The mean of these several frames was considered to be a single measurement. Regions of the array free of dead pixels were always used; bad pixels close to the star positions were replaced by linearly interpolated values.

Integration times were adjusted so that the peak signal in the core of the image was well below the point at which the linearity correction was substantial, viz., less than 2% (see below). Stars were observed at the minimum possible air mass. We tried to observe at least six, but no more than 10, E82 or part 1 standards each night. In no case were observations made when conditions were deemed to be marginal or nonphotometric. After all the reductions were completed for the nights believed to be photometric, data from two nights were discarded.

The seeing at Las Campanas was very good for this program, as is normal for the site. Typical image diameters on the 1 m telescope/C40IRC were $\approx 1\farcs1$, though because of the coarse pixel scale this is only an estimate. The generally excellent weather at Las Campanas allowed the observation of several stars a large number of times, and with an identical instrumental setup. The weather at Palomar was not as good as at Las Campanas during this program, and consequently the coverage and precision of the northern standards are not as high.

Several of the red stars are rather bright to be observed in the normal way, particularly at K or K_s. For these, the telescope was defocused enough to reduce the signal in the central few pixels by a factor of 2 or 3. Checks of signal versus focus showed that this procedure did not introduce spurious systematic offsets in the magnitudes.

3. DATA REDUCTION

3.1. *Linearization*

Data reduction was carried out with a set of scripts that call IRAF[3] routines. The first step was to correct for nonlinearity, as the Rockwell HgCdTe arrays display a nonlinear response that amounts to a few percent over the useful range of the detector. The linearity correction issue is endemic to all near-infrared arrays operated in a capacitive discharge mode. Linearization of the data is a crucial factor in spanning the 4 mag difference between the 7th magnitude E82 stars and the new ones near 11th magnitude, and special care was taken to measure and apply the linearity correction. Our systems do not use a mechanical shutter, so precise integration times were guaranteed by the use of hardware electronic timers, and are accurate at the few microsecond level. The frames are acquired in a double-correlated mode and thus a subtlety enters the situation.

[3] IRAF is distributed by the National Optical Astronomy Observatories, which are operated by the Association of Universities for Research in Astronomy, Inc., under cooperative agreement with the National Science Foundation.

TABLE 2

INFRARED STANDARD STARS

No.	*HST*	R.A. (J2000.0)	Decl. (J2000.0)	J	σ_m	N	H	σ_m	N	K	σ_m	N	K_s	σ_m	N	Note
9101	P525-E	00 24 28.3	07 49 02	11.622	0.005	16	11.298	0.005	16	11.223	0.008	10	11.223	0.005	17	4
9103	S294-D	00 33 15.2	−39 24 10	10.932	0.006	15	10.657	0.004	16	10.596	0.005	9	10.594	0.004	16	1
9104	S754-C	01 03 15.8	−04 20 44	11.045	0.005	17	10.750	0.005	17	10.693	0.010	8	10.695	0.005	17	2
9105	P530-D	02 33 32.1	06 25 38	11.309	0.010	8	10.975	0.006	8	10.897	0.006	7	10.910	0.005	8	1
9106	S301-D	03 26 53.9	−39 50 38	12.153	0.007	11	11.842	0.005	11	11.772	0.010	6	11.788	0.006	11	1
9107	P247-U	03 32 03.0	37 20 40	11.934	0.005	16	11.610	0.004	18	11.492	0.011	6	11.503	0.005	18	3
9108	P533-D	03 41 02.4	06 56 13	11.737	0.009	9	11.431	0.006	9	11.337	0.008	8	11.336	0.005	9	1
9109	S055-D	04 18 18.9	−69 27 35	11.552	0.002	65	11.326	0.002	65	11.255	0.027	2	11.269	0.002	66	2
9111	S361-D	04 49 54.6	−35 11 17	11.246	0.006	11	11.031	0.006	11	10.992	0.033	1	10.980	0.006	11	2
9113	S252-D	05 10 25.6	−44 52 46	11.059	0.005	16	10.766	0.005	16	10.708	0.034	1	10.713	0.005	16	2
9115	S363-D	05 36 44.8	−34 46 39	12.069	0.007	16	11.874	0.005	16	11.826	0.007	13	11.831	0.005	15	1
9116	S840-F	05 42 32.1	00 09 04	11.426	0.009	4	11.148	0.009	4	11.077	0.014	3	11.058	0.008	4	4
9118	S842-E	06 22 43.7	−00 36 30	11.723	0.011	3	11.357	0.009	3	11.264	0.016	2	11.261	0.010	3	3
9119	S121-E	06 29 29.4	−59 39 31	12.114	0.006	16	11.838	0.005	15	11.765	0.009	6	11.781	0.005	16	1
9121	S255-S	06 42 36.5	−45 09 12	11.719	0.004	27	11.434	0.004	27	…	…	0	11.372	0.004	26	2
9122	P161-D	07 00 52.0	48 29 24	11.680	0.006	8	11.408	0.006	8	11.356	0.013	3	11.352	0.006	8	3
9123	S427-D	06 59 45.6	−30 13 44	10.833	0.007	9	10.499	0.007	9	10.431	0.015	3	10.442	0.009	9	2
9125	S005-D	07 19 38.6	−84 35 06	10.885	0.007	9	10.598	0.006	9	10.514	0.013	4	10.522	0.008	9	2
9126	P309-U	07 30 34.5	29 51 12	11.876	0.013	2	11.522	0.014	2	…	…	0	11.450	0.022	2	3
9129	S209-D	08 01 15.4	−50 19 33	10.914	0.007	9	10.585	0.006	9	10.487	0.021	2	10.496	0.009	9	2
9131	P035-R	08 25 43.8	73 01 18	10.819	0.008	6	10.546	0.007	6	10.499	0.010	4	10.515	0.008	6	3
9132	S312-T	08 25 36.1	−39 05 59	11.949	0.006	16	11.669	0.005	16	11.608	0.004	14	11.609	0.004	17	1
9133	S495-E	08 27 12.5	−25 08 01	11.521	0.007	7	11.048	0.008	7	10.965	0.016	3	10.960	0.010	7	2
9134	P545-C	08 29 25.1	05 56 08	11.881	0.007	11	11.624	0.005	11	11.575	0.005	11	11.596	0.006	9	1
9135	S705-D	08 36 12.5	−10 13 39	12.362	0.010	4	12.098	0.011	4	…	…	0	12.040	0.014	4	2
9136	S165-E	08 54 21.7	−54 48 08	12.489	0.008	8	12.214	0.008	7	12.138	0.018	3	12.142	0.011	8	2
9137	S372-S	09 15 50.5	−36 32 34	11.153	0.007	7	10.891	0.007	7	10.830	0.019	2	10.836	0.010	7	2
9138	S852-C	09 41 35.8	00 33 12	11.354	0.006	9	11.041	0.006	9	10.981	0.015	3	10.982	0.008	9	4
9139	P091-D	09 42 58.7	59 03 43	11.683	0.008	5	11.338	0.007	5	11.276	0.011	3	11.282	0.010	5	3
9140	S262-E	09 45 42.8	−45 49 40	11.409	0.011	4	11.085	0.008	4	…	…	0	11.022	0.012	4	2
9141	S708-D	09 48 56.4	−10 30 32	11.081	0.008	6	10.775	0.008	6	10.715	0.035	1	10.718	0.010	6	2
9142	P212-C	10 06 29.0	41 01 26	11.993	0.006	9	11.729	0.005	9	11.686	0.009	5	11.697	0.007	9	3
9143	P550-C	10 33 51.8	04 49 05	12.344	0.007	12	12.121	0.005	12	12.067	0.006	12	12.081	0.005	12	1
9144	S264-D	10 47 24.1	−44 34 05	11.642	0.009	6	11.335	0.008	6	11.263	0.018	2	11.280	0.010	6	2
9145	P064-D	12 13 12.0	64 28 56	11.958	0.009	4	11.711	0.008	4	11.664	0.011	3	11.675	0.009	4	3
9146	S217-D	12 01 45.2	−50 03 10	11.323	0.007	17	11.002	0.005	18	10.931	0.003	15	10.936	0.004	18	1
9147	S064-F	12 03 30.2	−69 04 56	12.111	0.007	9	11.803	0.007	9	11.722	0.013	4	11.724	0.007	9	2
9148	P266-C	12 14 25.4	35 35 55	11.642	0.009	4	11.378	0.008	4	11.324	0.011	4	11.343	0.008	4	3
9149	S860-D	12 21 39.3	−00 07 13	12.213	0.007	14	11.917	0.006	14	11.861	0.005	12	11.865	0.005	14	1
9150	S791-C	13 17 29.6	−05 32 37	11.661	0.008	7	11.310	0.007	7	11.250	0.014	3	11.267	0.008	7	2
9152	P133-C	13 58 40.2	52 06 24	11.149	0.009	4	10.878	0.007	4	10.831	0.011	4	10.839	0.010	4	3
9153	P499-E	14 07 33.9	12 23 51	11.947	0.008	7	11.605	0.008	7	11.560	0.013	3	11.540	0.008	7	3
9154	S008-D	14 23 45.5	−84 09 58	11.232	0.007	8	10.990	0.007	8	10.904	0.009	7	10.915	0.008	8	2
9155	S867-V	14 40 58.0	−00 27 47	12.045	0.008	11	11.701	0.005	11	11.622	0.005	10	11.633	0.005	11	1
9156	P041-C	14 51 57.9	71 43 13	10.873	0.008	6	10.588	0.006	6	10.523	0.009	5	10.530	0.007	6	3
9157	S273-E	14 56 51.9	−44 49 14	11.341	0.007	16	10.924	0.005	17	10.851	0.004	15	10.849	0.004	17	1
9158	P272-D	14 58 33.1	37 08 33	11.640	0.008	6	11.277	0.006	6	11.210	0.008	6	11.223	0.007	6	3
9160	S870-T	15 39 03.5	00 14 54	10.914	0.008	6	10.701	0.008	6	10.649	0.010	5	10.659	0.009	6	2
9162	P177-D	15 59 13.6	47 36 40	12.258	0.012	3	11.924	0.008	3	11.857	0.013	3	11.868	0.012	3	3
9164	P565-C	16 26 42.7	05 52 20	12.180	0.007	8	11.895	0.006	8	11.842	0.007	6	11.844	0.006	7	1
9166	P330-E	16 31 33.6	30 08 48	11.816	0.007	9	11.479	0.005	9	11.419	0.007	9	11.429	0.006	9	3
9169	P138-C	17 13 44.5	54 33 21	11.355	0.007	8	11.118	0.005	8	11.075	0.008	8	11.080	0.007	8	3
9170	S875-C	17 27 22.2	−00 19 25	11.132	0.005	13	10.835	0.005	13	10.739	0.006	13	10.744	0.005	13	4
9172	S279-F	17 48 22.6	−45 25 45	12.477	0.009	8	12.118	0.006	8	12.026	0.006	8	12.031	0.006	8	1
9173	S024-D	18 18 46.2	−80 06 58	11.039	0.007	8	10.778	0.007	8	10.693	0.009	7	10.711	0.008	8	2
9175	S071-D	18 28 08.9	−69 26 03	12.252	0.006	11	11.916	0.007	11	11.834	0.011	6	11.839	0.007	11	2
9177	P182-E	18 39 33.7	49 05 38	12.104	0.005	15	11.764	0.004	15	11.688	0.006	15	11.696	0.005	15	3
9178	S808-C	19 01 55.4	−04 29 12	10.966	0.007	9	10.658	0.008	9	10.566	0.014	4	10.575	0.008	9	2
9181	S234-E	20 31 20.4	−49 38 58	12.464	0.011	5	12.127	0.008	5	12.095	0.007	4	12.070	0.007	5	1
9182	S813-D	20 41 05.1	−05 03 43	11.479	0.005	15	11.142	0.005	15	11.082	0.010	7	11.085	0.005	15	2
9183	P576-F	20 52 47.3	06 40 05	12.247	0.004	23	11.940	0.004	23	11.873	0.007	14	11.880	0.005	23	4
9185	S889-E	22 02 05.7	−01 06 02	12.021	0.005	18	11.662	0.004	18	11.586	0.012	8	11.585	0.005	18	4
9186	S893-D	23 18 10.0	00 32 56	11.403	0.009	7	11.120	0.006	7	11.045	0.006	6	11.055	0.006	7	1
9187	S677-D	23 23 34.4	−15 21 07	11.857	0.003	39	11.596	0.003	39	11.538	0.009	10	11.542	0.003	39	2
9188	P290-D	23 30 33.4	38 18 57	11.634	0.005	15	11.337	0.004	15	11.257	0.008	8	11.262	0.006	15	3

NOTE.—(1) These 17 new standards were selected to lie close on the sky to an E82 standard. Measured on the Las Campanas 1 m Swope Telescope using IRCAM and referred directly to several E82 standards on each night. (2) Measured on the Las Campanas 1 m Swope Telescope using the C40IRC and referred to the code 1 (part 1) new standards. (3) Measured on the Palomar Observatory 1.5 m Telescope using the P60IRC and referred to the equatorial code 1 (part 1) new standards. (4) Measured on both telescopes; results averaged.

TABLE 3

RED STARS

Name	R.A. (J2000.0)	Decl. (J2000.0)	J	σ_m	N	H	σ_m	N	K	σ_m	N	K_s	σ_m	N	Note
BRI 0021	00 24 24.6	−01 58 22	11.835	0.008	6	11.086	0.007	6	10.552	0.010	6	10.561	0.008	6	4
T832-38078	03 04 02.0	00 45 52	11.833	0.010	5	11.248	0.008	5	10.890	0.013	5	10.913	0.008	5	4
LHS 191	04 26 20.1	03 36 40	11.621	0.013	2	11.058	0.012	2	10.667	0.020	2	10.717	0.016	2	2
IRAS 537 W	05 40 10.5	−07 27 38	12.974	0.009	4	11.032	0.009	4	9.981	0.013	3	10.013	0.011	4	2
IRAS 537 S	05 40 15.4	−07 28 46	13.855	0.012	3	12.087	0.009	3	10.972	0.014	3	11.035	0.012	3	2
LHS 2026	08 32 30.5	−01 34 37	12.066	0.006	10	11.497	0.005	10	11.129	0.007	10	11.156	0.008	10	2
LHS 2397a	11 21 49.2	−13 13 10	11.897	0.008	6	11.190	0.007	6	10.691	0.008	6	10.709	0.010	6	2
cskd-8	12 31 13.3	−63 40 21	11.741	0.010	4	9.913	0.010	4	9.151	0.011	4	9.137	0.013	4	2
cskd-9	12 31 16.7	−63 40 11	11.372	0.010	4	9.788	0.010	4	9.161	0.011	4	9.154	0.013	4	2
cskd-12	12 31 30.0	−63 42 41	11.585	0.007	8	9.506	0.005	8	8.617	0.007	8	8.608	0.007	8	2
cskd-15a	12 31 44.5	−63 49 08	10.879	0.010	4	9.286	0.007	4	8.625	0.010	4	8.617	0.011	4	2
cskd-16	12 31 57.8	−63 42 21	11.986	0.011	3	9.982	0.008	3	9.137	0.011	3	9.124	0.010	3	2
cskd-18	12 31 59.2	−63 41 42	9.365	0.010	3	9.058	0.008	3	8.999	0.011	3	8.992	0.010	3	2
cskd-20	12 32 04.0	−63 43 46	9.903	0.011	3	8.590	0.008	3	8.089	0.011	3	8.077	0.010	3	2
cskd-21	12 32 10.9	−63 43 16	10.382	0.006	9	9.918	0.006	9	9.647	0.007	9	9.658	0.007	9	2
cskd-34	12 31 23.6	−63 46 45	12.494	0.015	2	10.537	0.014	2	9.677	0.016	2	9.668	0.019	2	2
cskd-37	12 31 30.1	−63 47 12	12.489	0.015	2	10.415	0.014	2	9.528	0.016	2	9.513	0.019	2	2
cske-23	12 31 56.0	−63 37 43	10.624	0.008	5	8.762	0.006	5	7.917	0.008	5	7.889	0.008	5	2
cskf-12	12 31 30.1	−63 51 03	9.671	0.008	5	8.858	0.007	5	8.561	0.009	5	8.561	0.008	5	2
cskf-13a	12 31 39.5	−63 51 03	10.631	0.010	4	9.861	0.009	4	9.486	0.011	4	9.506	0.011	4	2
cskf-14a	12 31 45.9	−63 49 36	10.095	0.008	5	8.851	0.007	5	8.387	0.009	5	8.361	0.008	5	2
T868-53850	15 00 26.4	−00 39 29	11.589	0.008	5	10.993	0.008	5	10.633	0.009	5	10.657	0.012	5	2
T868-110639	15 10 17.0	−02 41 05	12.612	0.009	5	11.865	0.010	5	11.336	0.009	5	11.353	0.011	5	2
L134	15 53 38.4	−04 39 04	11.408	0.009	4	9.627	0.010	4	8.875	0.011	4	8.898	0.013	4	2
Oph N9	16 27 13.3	−24 41 34	17.549	0.022	2	12.389	0.011	2	9.527	0.014	2	9.620	0.018	2	2
L547	18 51 15.6	−04 16 02	11.872	0.010	4	9.831	0.011	4	8.888	0.014	4	8.870	0.016	4	2
BRI 2202	22 05 36.0	−11 04 27	11.652	0.010	4	11.083	0.009	4	10.721	0.013	4	10.736	0.011	4	4

NOTE.—See Table 2 for key to notes.

Once the array reset voltage has been lifted, the array begins detecting light, i.e., before the first integration of the two that compose a double-correlated read. In principle then, the voltage measured at the first read is already slightly nonlinear. Depending on the length of the exposure and on the brightness of the star, a simple low–light-level linearity correction factor will underestimate the correction necessary. In order to account for this effect a simple algebraic model of the dependence of output upon input was developed, and the unknown factor C in the expression $I(\text{out}) = I(\text{in})\ [1 + CI(\text{in})]$ was found by measuring the output as a function of input light level of the illuminated dome as the exposure time was varied. The parameter C is actually a function of the ratio of the integration time to the time elapsed from time zero to beginning of the first read. The linearity correction is about 4% over the whole range of signal out of the array, for the long integration time case. We minimized the correction by keeping the corrected central pixel signal levels less than 70% of "maximum." Typically about 70% of the light in the stellar image profiles falls outside the central one or few pixels where the linearity correction matters the most. Thus on average the corrections for the E82 stars were about 1%.

The accuracy of the linearization procedure for parts 2 and 3 of the program became almost irrelevant, because all the stars have comparable magnitudes, around 11th at K, and consequently both the signal levels and integration times were comparable for the E82 standards and the new ones.

3.2. *Further Processing*

After linearization, sets of frames at a given telescope position were averaged with a (5) σ clipping algorithm turned on; this rejected pixel values saturated by cosmic rays. Average dark frames were subtracted from the data frames, which were then divided by the normalized flat-field pictures. Sky frames were computed for each (averaged) frame in a sequence, as follows. Suppose the star image was placed at four locations on the array. The sky to be used for the first frame was computed from the other three averaged pictures. Files of field star locations were kept for each star, and these locations were used to automatically clean the frames of all stars (including the target) before averaging the three to produce the first sky frame. This step guaranteed that very clean sky frames were always used. The signal levels of the sky frame and the star frame to which it pertains were then compared. In general, these levels (taken as the modes) were not identical, because the sky background can be variable at the few percent level, on timescales as short as seconds. The sky frame was scaled so that its resulting mode was equal to that of the star frame. Subtraction then produced a corrected star frame whose residual sky level was very close to zero. Any deviations from zero are caused, we believe, by uncertainty in the estimation of the modes, and by second-order variations in the fringing pattern, which is most pronounced in the H band. Aperture photometry was performed on versions of the sky-subtracted frames that were cleaned of nearby stars; an aperture 10″ in diameter was used. This rather large aperture contributed extra sky noise, but reduced the systematic effects of seeing variations. The (near-zero) sky was subtracted one last time by taking the median value within an annular aperture around the star.

4. RESULTS

4.1. *New Standard-Star Magnitudes*

Table 2 lists the results for the *HST* stars of the program. Entries are listed by a star designation number adopted for

convenience; the *HST* designations are also given. Our numbers are not sequential, because some stars were dropped from the program. The uncertainties listed with each magnitude are 1 σ of the mean, calculated according to the precepts outlined in § 4.3. The columns labeled N give the number of measurements for each filter. Table 3 contains the data for the red stars.

4.2. *Positions and Finding Charts*

The positions listed for the stars in Table 2 were taken from Lasker et al. (1988), the Coalsack star positions are from Jones et al. (1980), and the other red star positions were checked using the set of *HST* CD-ROMs.

Figure 1 presents H-band finding charts for all the program stars. North is up, east is to the left, and each chart is 106″ on a side. Three of the red stars, LHS 191, LHS 2026, and LHS 2397a, have proper motions larger than 0.″5 per year. Table 4 lists the proper-motion vectors from Luyten (1979); the epoch for these three charts is 1996.90.

Two fields require some explanation. The Lynds 547 dark cloud contains many red stars, one of which we selected on the basis of color and K magnitude. The extremely red star Oph N9 in the Rho Ophiucus dark cloud was suggested by Elias. It corresponds to star BKLT 162713-244133 of Barsony et al. (1997), and to source number 232 of Greene & Young (1992).

4.3. *Uncertainties*

The most important uncertainties arise from the cameras, detectors, and the atmosphere. Nonideal pixel scales, imperfections in linearization, flat-fielding, removal of pixels affected by cosmic rays, and calculation of the sky frames all contribute small amounts to the uncertainties. Low-level variations in atmospheric transparency and in water vapor content are probably responsible, however, for most of the dispersion in the measured instrumental magnitudes for standard stars throughout a night. It has been our practice not to try to solve for air mass corrections night by night, as this can lead to spurious values for coefficients if the extinction is variable and nongray. The latter is relevant at the filter passband edges, where water vapor influences the effective width of the passband. We have adopted canonical air mass corrections of 0.10, 0.04, and 0.08 mag per air mass (at J, H, and K_s, respectively) and measured all standards and unknowns over the smallest possible range of air mass, typically 0.2. Our adopted corrections are rather close to the average values measured in the northern 2MASS survey, viz., 0.11, 0.03, and 0.06 mag per air mass (R. Cutri 1998, private communication).

The 1 σ_m (standard deviation of the mean) uncertainties for each new standard in part 1 are given in Tables 2 and 3. In calculating the weights for each individual measurement, it was assumed that the E82 stars have effectively zero uncertainty. This assumption certainly seems justified, as the highest quality E82 standards were usually measured many times. For a given night, the dispersion in the instrumental constant (i.e., the instrumental magnitude corresponding to some known photon arrival rate) was used to compute the uncertainty for each measurement. This uncertainty is an indicator of the quality of the night; the values over all nights, both average and median, are given in Table 5. To these were added the σ_m of the separate measurements on the array. The recipe for the stars measured in parts 2 and 3 was to carry into the uncertainty in the night constant a contribution from the final uncertainties in each of the part 1 standards. Thus the second set of new standards—codes 2, 3, and 4 in Tables 2 and 3—are not formally as well measured as those of the first set.

Implicit in Table 5 is that high-precision stellar measurements in the near-infrared wavebands are not difficult to make, provided sufficient care is taken, particularly in the production of sky frames.

The individual data points for a given star in a given passband were averaged giving $1/\sigma_m^2$ weight to each, so for individual data points x_i, the average $\langle x \rangle$ is

$$\langle x \rangle = \frac{\sum_i x_i/\sigma_{m,i}^2}{\sum_i 1/\sigma_{m,i}^2} .$$

The formal uncertainty in the tabulated magnitudes is then given by

$$\sigma_{m,x}^2 = \frac{1}{\sum_i 1/\sigma_{m,i}^2} .$$

This uncertainty is a function of the σ_m's alone, which must therefore be well known. Figure 2 illustrates how the weighting scheme worked in practice; the individual data points and their uncertainties are shown for star 9187 = HST S677-D. The horizontal lines are the weighted means with arbitrary vertical shifts applied for clarity. The dispersion around the mean value appears to be too small for the error bars. Plots of the integral distributions of the parameter $(\mathrm{mag}_i - \langle \mathrm{mag} \rangle / \sigma_m)$ for each passband show that for J, H, and K_s about 95% of the data points lie within 1 σ_m of the mean value, compared to 67% for a normal distribution. This is the case for essentially every star in the sample: the uncertainties in Tables 2 and 3 appear to be between 60% and a factor of 2 too large, formally speaking. The explanation for this must be that taking the *dispersion* for the standard stars' data for a given night overestimates the uncertainties. It is often the case at Las Campanas that a high inversion layer falls during the first few hours of the night and this produces a (small) monotonic increase in

TABLE 4

PROPER MOTIONS FROM LUYTEN 1979

Star	Epoch	μ (arcsec yr^{-1})	P.A. (deg)
LHS 191	1996.9	1.033	186.4
LHS 2026	1996.9	0.500	161.0
LHS 2397a.....	1996.9	0.515	261.0

TABLE 5

CONTRIBUTIONS TO STATISTICAL WEIGHTS

Parameter	J	H	K	K_s
No. of standards/night:				
Average.....	6.6	6.5	6.7	6.5
Median	7	7	6	7
Dispersion of standards (mag):				
Average.....	0.017	0.018	0.023	0.022
Median	0.016	0.017	0.020	0.020
No. of array locations:				
Average.....	3.8	3.8	3.5	3.8
Median	3	3	3	3
Dispersion on array (mag):				
Average.....	0.012	0.016	0.020	0.021
Median	0.012	0.014	0.019	0.019

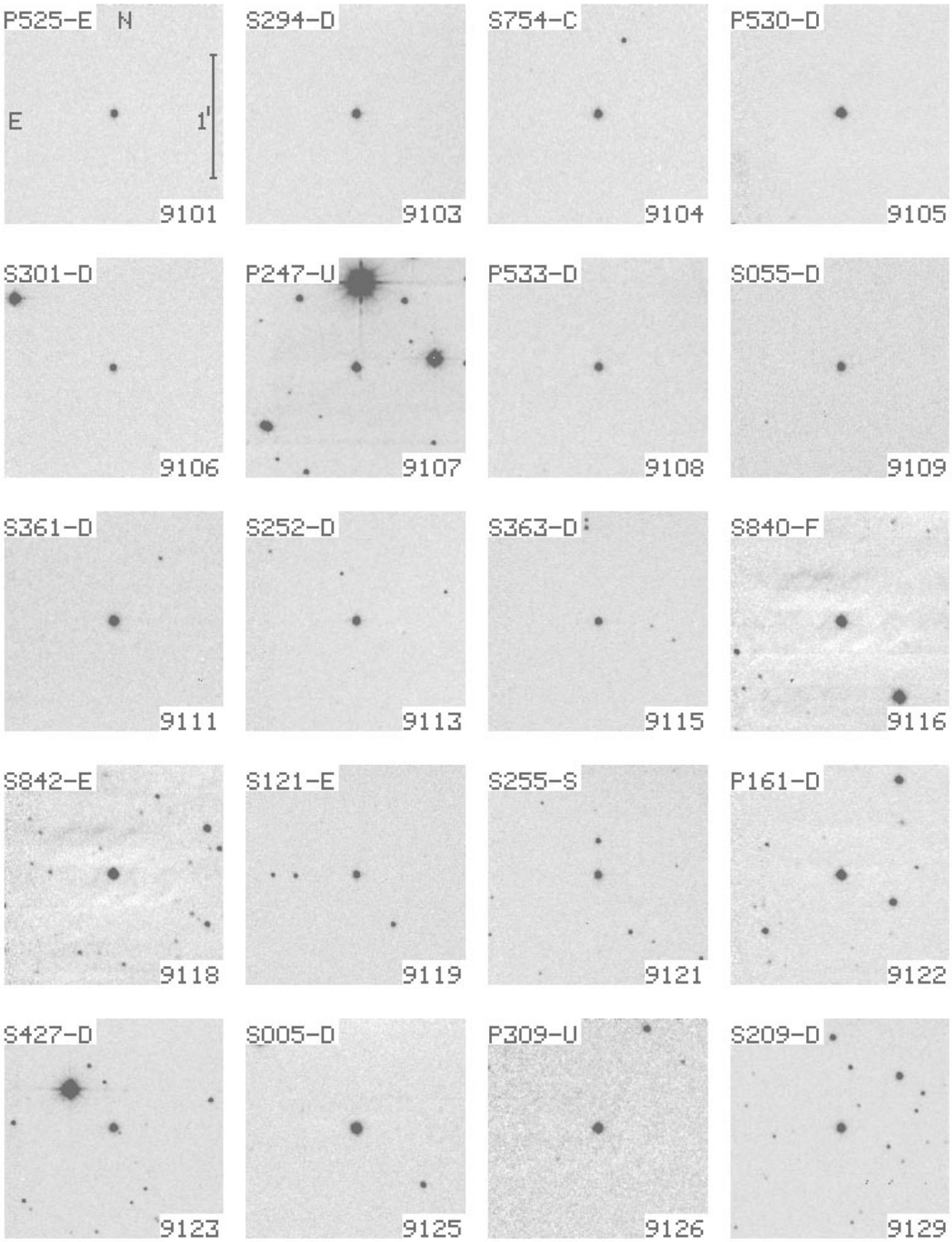

FIG. 1.—Finding charts for faint standard stars and for red stars. Charts were made from H-band pictures at scales of either 0.″60 or 0.″62 pixel^{-1}, and are 106″ on a side. North is up, east is to the left, and the 1′ scale bar shown once on each panel is the same for all charts. The target *HST* star is centered, while some of the red stars are labeled or indicated.

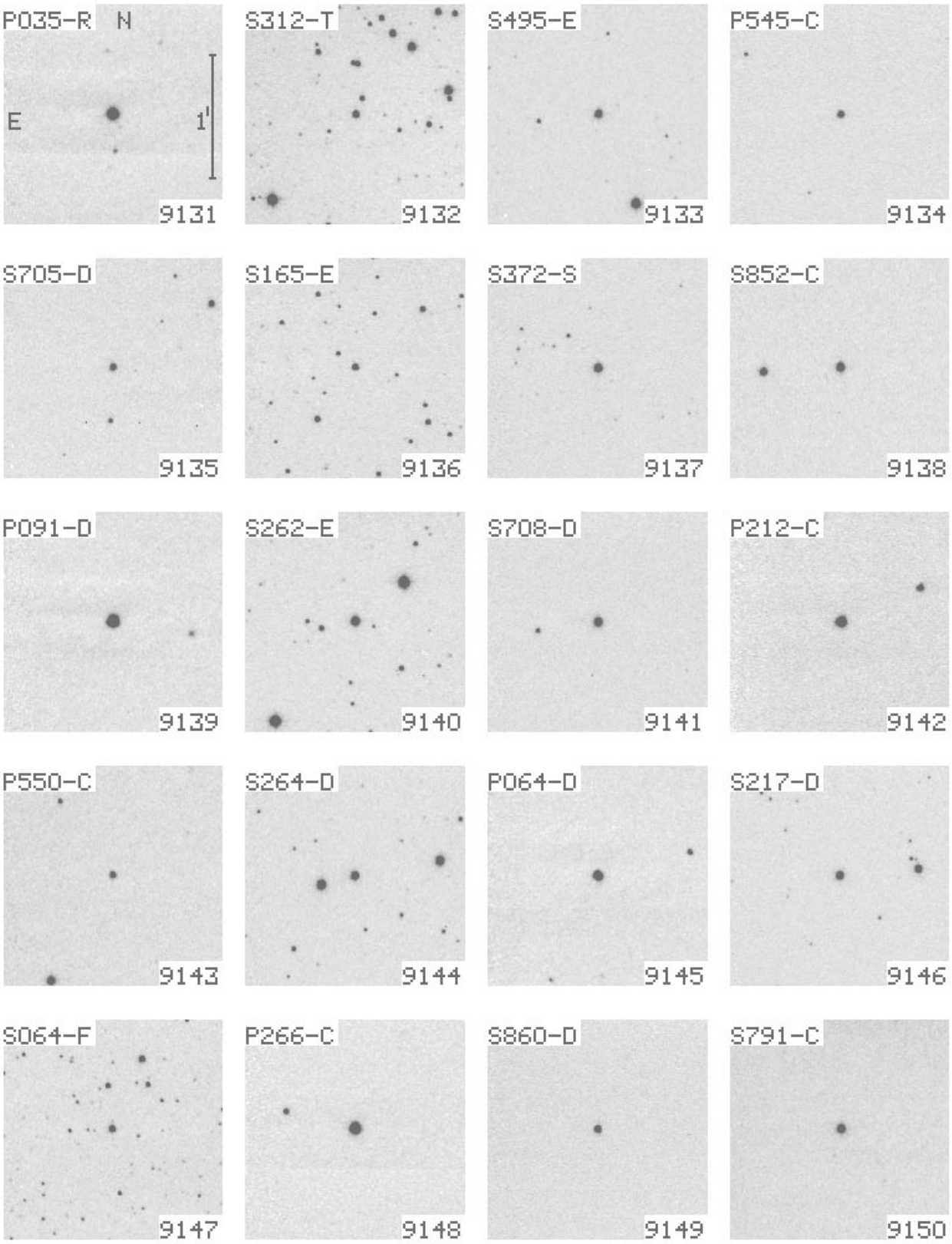

FIG. 1.—*Continued*

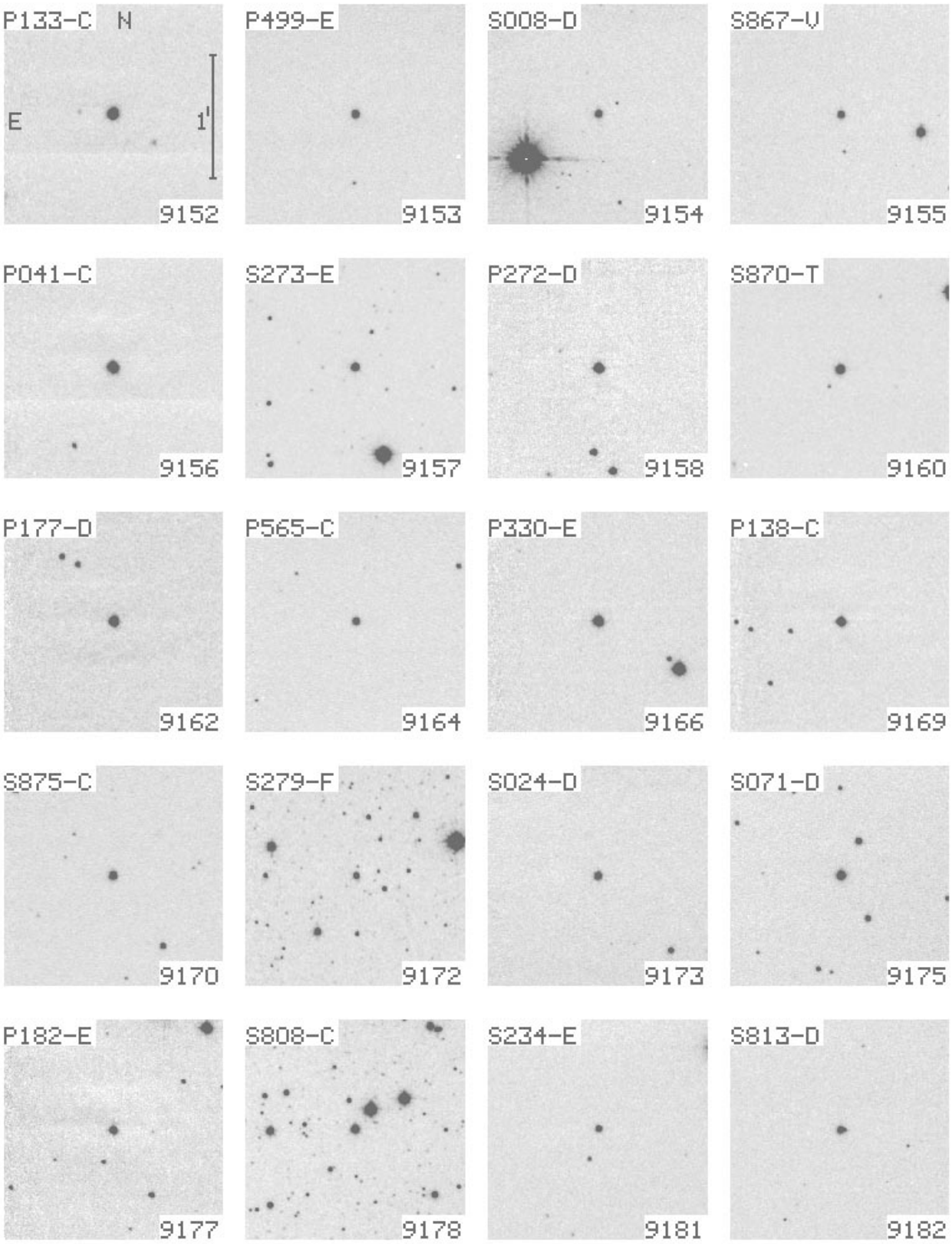

FIG. 1.—*Continued*

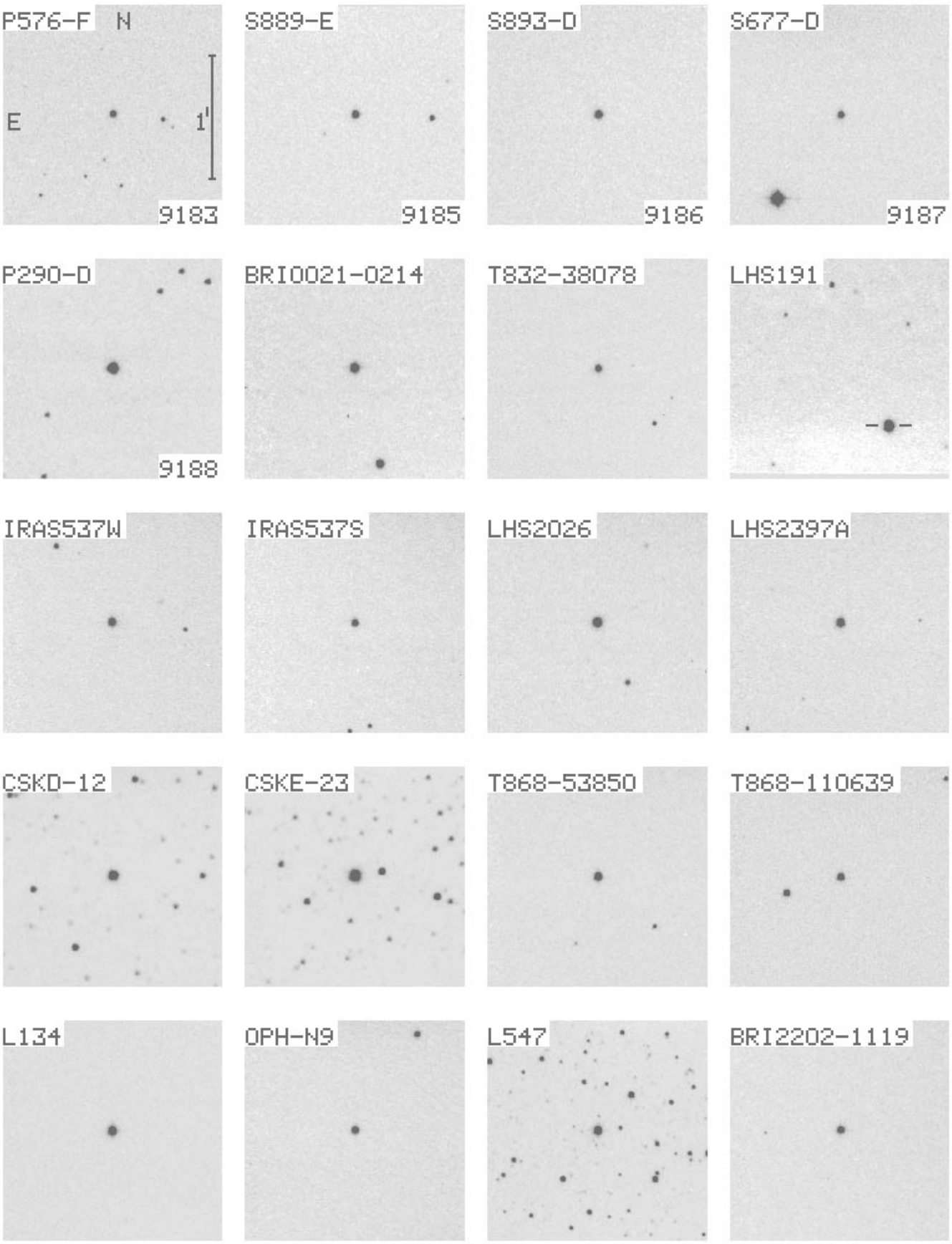

FIG. 1.—*Continued*

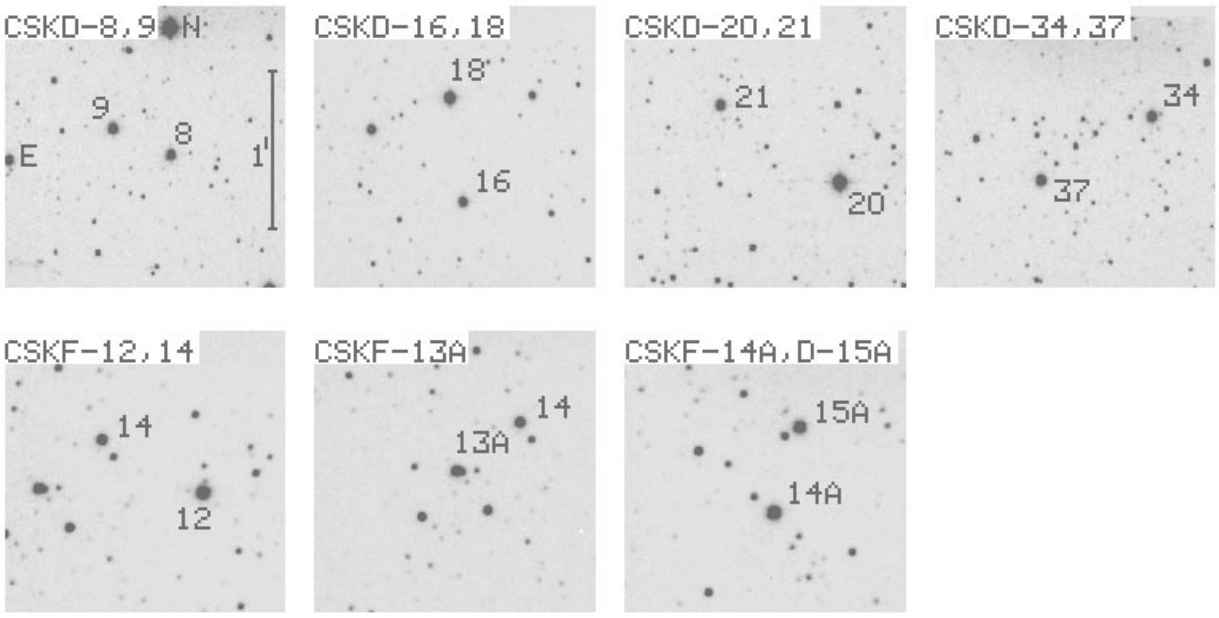

FIG. 1.—*Continued*

transparency. Most of the data obtained under these conditions may then be better than indicated by the dispersion for the whole night. This explanation notwithstanding, we advocate using the uncertainties given in the tables, should they be needed.

4.4. *Variability*

The color selection criteria of the *HST* guide stars suggests that variability should be rare or absent in our sample. In no case was any star found to be variable in any passband, over the 3 year span of the observations. Figure 2, which shows a typical set of uncertainties, also illustrates the typical case for nonvariability.

The red stars have *not* been extensively monitored for variability, and while the colors should vary less than the magnitudes, caution should be used. Some of Coalsack stars do appear to be varible, as discussed by E83 and below, in § 5.3. Recently, R. Cutri (1998, private communication) has communicated 2MASS results on the red star in the L547 field that indicate that it might be variable. The present colors agree with those of 2MASS, but the magnitude of the star appears to have changed by about 0.07 mag.

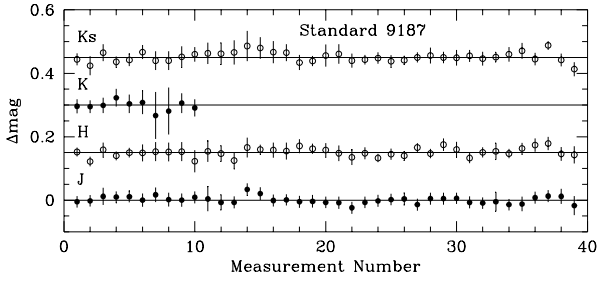

FIG. 2.—Individual data points and 1 σ_m uncertainties for the new standard number 9187 = HST 677-D. The *x*-axis is observation number, and the *y*-axis shows the deviations from the mean values, with arbitrary offsets applied for clarity. The dispersions about the mean values appear too small compared with the uncertainties, indicating that the latter are overestimated.

Barsony et al. (1997) list the following magnitudes for Star Oph N9: $J > 17.0$, $H = 12.54$, and $K = 9.58$, compared with our data: $J = 17.55$, $H = 12.39$, $K = 9.53$. These magnitude differences may well result from differences in the effective wavelengths of the two photometric systems, and are not surprising considering the extremely red colors of this star.

5. COMPARISONS

5.1. *Las Campanas/Palomar*

Six equatorial *HST* stars and six red stars were measured from both Las Campanas and from Palomar. The average differences are between 0.01 and 0.02 mag for each filter, but the average observational uncertainties for the Palomar data are rather large, and none of the differences is formally significant.

5.2. *Las Campanas/UKIRT*

Early in part 1 of this program, measurements were made of several UKIRT standard stars (Casali & Hawarden 1992). The primary purpose was to check our magnitude scale using a completely independent data set. Table 6 shows our UKIRT star data reduced using the Table 2 values for the new standards. The main result is that the *K* magnitudes agree fairly well, and consequently that we have no reason to suspect a linearity error at the 0.01 mag level or better, between 7th and 12th magnitude at *K*. This statement rests on the *K* magnitudes, as color differences might be expected for *J* and *H*.

A second result is that our $J-K$ color system agrees rather well with that of UKIRT, although this is not a strong result as neither the number of stars, the color range, nor the uncertainties are really adequate. There appears to be a 2 σ offset between our $H-K$ color systems, but this is not a cause for concern, given the limited number of comparisons.

TABLE 6

LAS CAMPANAS/UKIRT COMPARISON

UKIRT Standard	Nights	LCO Photometry			UKIRT Values		
		K	$J-K$	$H-K$	K	$J-K$	$H-K$
5	3	12.350 ± 0.015	0.021 ± 0.025	0.047 ± 0.025	12.342	−0.007	−0.002
7	3	10.948 ± 0.015	0.169 ± 0.025	0.038 ± 0.025	10.940	0.165	0.037
17	2	12.316 ± 0.020	0.346 ± 0.030	0.037 ± 0.030	12.270	0.411	0.073
18	8	10.544 ± 0.015	0.310 ± 0.020	0.065 ± 0.020	10.522	0.292	0.031
24	4	10.770 ± 0.025	0.145 ± 0.030	0.034 ± 0.030	10.753	0.151	0.019
34	5	12.970 ± 0.020	−0.090 ± 0.030	−0.034 ± 0.030	12.989	−0.170	−0.070
35	1	11.693 ± 0.030	0.499 ± 0.040	0.130 ± 0.040	11.757	0.474	0.089

The new infrared standard values of Hunt et al. (1998) were established relative to the UKIRT system stars. The differences at K shown in Table 6 suggest that the UKIRT values, and consequently those of Hunt et al., may contain small systematic and/or random errors. Comparisons of additional UKIRT stars measured by the 2MASS project (R. Cutri 1998, private communication) support this contention, but are not extensive enough as yet to permit a definitive comparison.

5.3. *Coalsack Star Data and Color Transformations*

Elias et al. (1983, henceforth E83) presented a comparison of the CIT/CTIO and Anglo-Australian Observatory (AAO) infrared photometric systems based in part upon measurements of red stars in the Coalsack Nebula. The purpose of the comparison was to establish color transformations that could be used to place data from one system onto the other. We have likewise measured a number of Coalsack stars, in order to get approximate transformations, but the comparisons are not exhaustive. We measured several stars not directly measured on the CIT/CTIO system, so we have transformed the necessary Jones et al. (1980) data using the E83 equations to compile the magnitudes, colors, and differences for 14 Coalsack stars. Figure 3 plots the correlations and Table 7 gives the least-squares fits. The weights for each data point were derived from the uncertainties in Table 3. The outlying star on the plots is cskd-8, whose data are transformed from the AAO system; it has been ignored in the fits.

The $J-K$ and $J-H$ figures show a rather strong color term, which is caused by the J filters, as there is only a small color term for $H-K$, and no systematic dependence of K magnitude on color. The sense of the J-dependent color differences between the CIT/CTIO and the present LCO system is that systematically redder stars appear even redder on the LCO system, and at a level intermediate between the CIT/CTIO versus AAO systems. This is qualitatively consistent with expectation, as the CIT/CTIO system used a Silicon Fabry lens to image the telescope entrance pupil onto the InSb detector. The refractive index and transmission of silicon change rapidly across the J band, and the net result is that the effective wavelength of the CIT/CTIO J filter lies to the red of that of the LCO system. (Neither the AAO nor the LCO systems use silicon optics.) A red star will appear brighter at J on the CIT/CTIO system, and thus $J-H$ or $J-K$ bluer, compared with the LCO system. It should also be noted that the color difference between the LCO and CIT/CTIO systems is defined to be zero for the A0 standard stars of E82. The formal $J-H$ and $J-K$ linear fits do not pass through (0, 0), as they should, and thus the linear relationships are defined only for $J-H > 0.35$ and $J-K > 0.45$. The $H-K$ correlation was forced to pass through (0, 0), as this appeared to be consistent with the data. The K-magnitude comparison shows considerable scatter, but as E83 noted, color variations should be smaller, and indeed the tightness of the correlations bears this out.

Our color transformation measurements are not extensive enough to be definitive. The advent of the 2MASS database has made this point rather moot, however. We expect that color transformations of the sort needed for future near-infrared astronomy will be referred to stars with very well-measured colors in the 2MASS catalog.

5.4. *K versus K_s*

The zero point of the K_s magnitudes in our system is set by assuming that $K_s = K$ for the A0 E82 standards. The data in Table 3 show considerable scatter in the relationships between $K_s - K$ and color (for example, $J-K$). This results from the presence (or lack thereof) of stellar CO-band absorption, which affects the K filter much more than the K_s filter. If colors and transformations between K and K_s for giants, dwarfs, or other objects are required, the filter profiles in the Appendix can be used.

We are indebted to a large number of people who contributed to this program. The scientists and engineers at Rockwell—Kadri Vural, Duc Bui, and Scott Cabelli—have been exceedingly helpful as we brought three infrared

TABLE 7

SYSTEM COMPARISON: LAS CAMPANAS VERSUS CIT/CTIO

Color	Conversion
$(J-H)_{CIT}$	$(0.936 \pm 0.009)(J-H)_{LCO} + (0.029 \pm 0.013)$; $(J-H)_{LCO} > 0.35$
$(J-K)_{CIT}$	$(0.954 \pm 0.007)(J-K)_{LCO} + (0.015 \pm 0.014)$; $(J-K)_{LCO} > 0.45$
$(H-K)_{CIT}$	$(0.974 \pm 0.020)(H-K)_{LCO} \pm (0.013)$

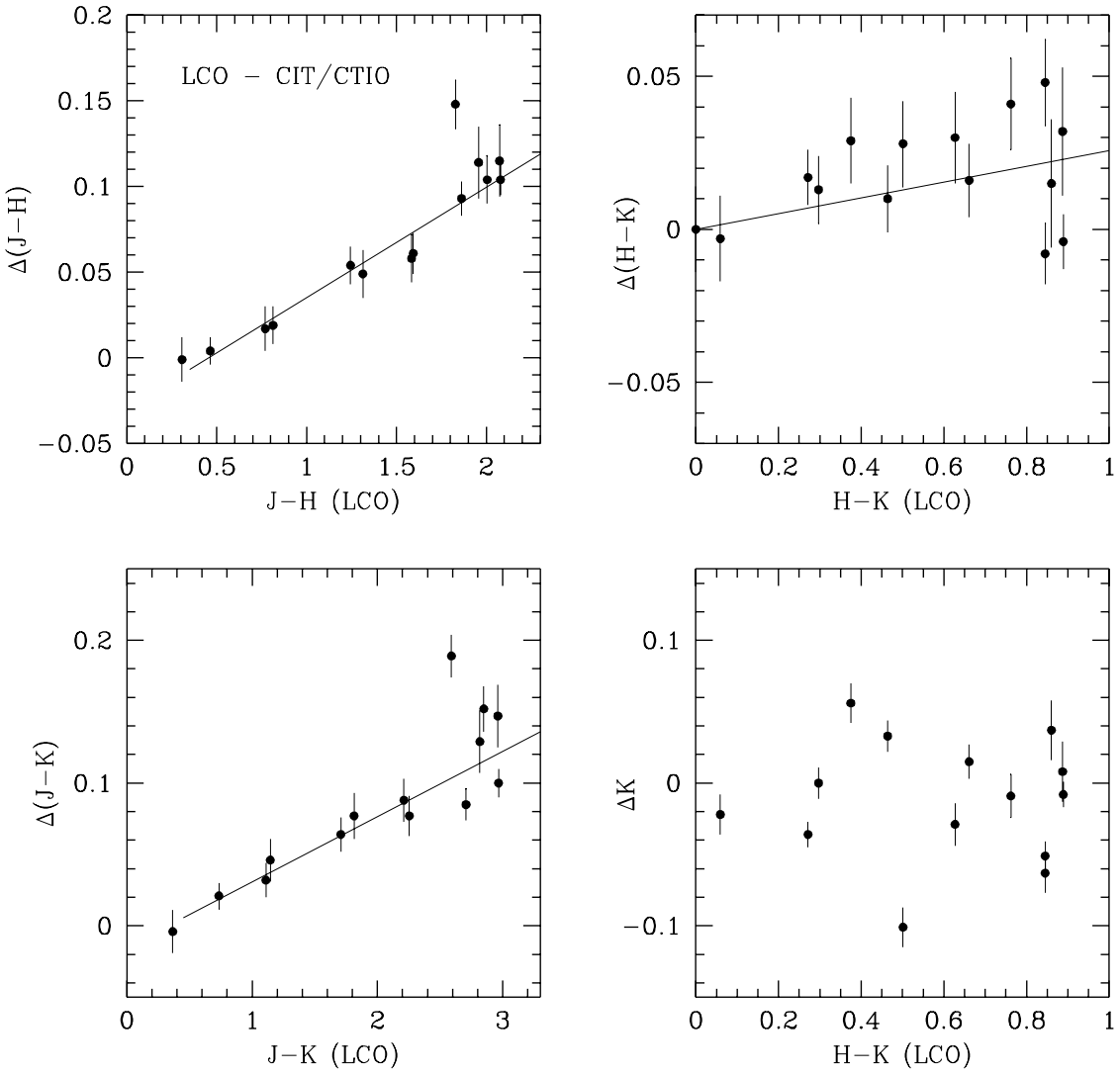

FIG. 3.—The differences in color between the present system and those of E83, with some data transformed from Jones et al. (1980), for 14 stars in the Coalsack Nebula. The color differences are in the sense LCO minus CIT/CTIO. The linear fits shown are listed in Table 7. Variability of the stars at K accounts for the large scatter in ΔK (see E83 for discussion).

detector/camera systems to completion. Mario Mateo and Barry Madore made a number of measurements in part 1 of the program. The support personnel at Las Campanas and Palomar Observatories were helpful and professional in every respect. The position of L547 was determined using *r*- and *i*-band charts kindly provided by the Royal Observatory Edinburgh group, and has been verified in early results from the 2MASS survey (R. Cutri 1998, private communication), for which we thank Roc Cutri. We also thank Jay Elias for his interest in this program and for providing advice regarding the selection of the red stars. Part of the funding for this project was provided by the Space Telescope Science Institute.

APPENDIX

FILTERS AND EFFECTIVE PASSBANDS

We endeavored to use identical filters in each of our three cameras, but this was not always feasible. Figure 4 shows the transmission functions of the filters and a quantum efficiency curve for a typical Rockwell HgCdTe detector. The marked decline in quantum efficiency toward shorter wavelengths is not necessarily as pronounced for the three detectors used for this program. The filter transmission functions are appropriate for normal incidence and operation at 77 K.

The K_s ("K short") filter was developed by M. Skrutskie. It was specifically designed to reduce the thermal background at ground-based sites that do not typically experience very cold ambient temperatures. It is not the same as the K' ("K prime") filter in use at Mauna Kea Observatory (Wainscoat & Cowie 1992). The background reduction is a factor of 2 during typical observing conditions at Palomar and Las Campanas.

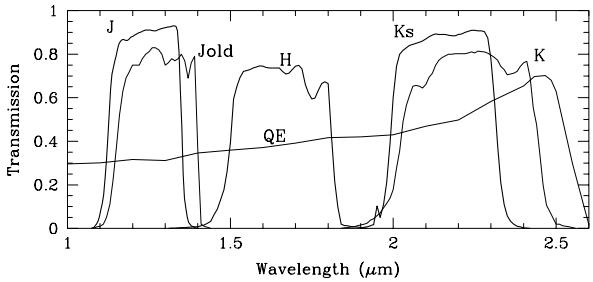

FIG. 4.—Filter transmissions and a typical NICMOS3 quantum efficiency curve for this system. The curve labeled *J* is the new filter used in parts 2, 3, and 4 of the program. *J*old is the old filter used in part 1. The transmissions are for normal incidence at the filter/detector operating temperature of 77 K. Tables 8 through 11 contain the numerical data for the filter curves alone. The very small shifts due to filter tilts are discussed in the text.

The *J* filter, obtained from Optical Coating Laboratories, Inc. (Santa Rosa, California), was specially designed for this program. The goal was to locate the edges of the passband so that transmission variations in the atmospheric water vapor bands would introduce less scatter into the data, while not reducing the throughput too severely. The task of designing a new *J* filter has been considered in some detail by Young, Milone, & Stagg (1994), and by Simons (1996).[4] Our approach was less quantitative than either of these studies; we specified the passband while visually inspecting a nominal atmospheric transmission curve. The variations in transmission are sharply dependent on wavelength and atmospheric water vapor content, as can be seen in the *J*-band figures in Young et al. (1994). Our expectations of an improvement over our previous filters was borne out. Table 5 shows that the typical dispersion in the system transmission throughout a night is no larger at *J* than at *H*.

Direct comparisons of magnitudes for our old and new *J* filters were made for several stars during several nights; no significant differences were found and the two filters are consequently treated as if they have identical effective wavelengths. This is not unexpected for the relatively neutral-colored stars that define the present system, given the transmission data shown in Figure 4.

Tables 8 through 11 list the data presented in Figure 4. From these one can compute accurate synthetic colors for model energy distributions.

For parts 2, 3, and 4 of this program, in which the new P60IRC and C40IRC cameras were used, the filter passbands were slightly altered from those presented in Figure 4 and Tables 8 through 11. The filters were tilted by 5° in order to deflect ghost images away from the primary image. The passband curves thus shift to shorter wavelengths by the following amounts: *J*,

TABLE 8

TRANSMISSION OF NEW *J* FILTER

λ	T	λ	T	λ	T	λ	T	λ	T
1.08.....	0.000	1.15.....	0.785	1.22.....	0.892	1.29.....	0.910	1.36.....	0.140
1.09.....	0.025	1.16.....	0.850	1.23.....	0.900	1.30.....	0.915	1.37.....	0.045
1.10.....	0.065	1.17.....	0.860	1.24.....	0.905	1.31.....	0.918	1.38.....	0.015
1.11.....	0.135	1.18.....	0.860	1.25.....	0.905	1.32.....	0.927	1.39.....	0.000
1.12.....	0.320	1.19.....	0.865	1.26.....	0.900	1.33.....	0.925		
1.13.....	0.555	1.20.....	0.875	1.27.....	0.902	1.34.....	0.875		
1.14.....	0.720	1.21.....	0.883	1.28.....	0.906	1.35.....	0.495		

TABLE 9

TRANSMISSION OF *H* FILTER

λ	T	λ	T	λ	T	λ	T	λ	T
1.31.....	0.000	1.44.....	0.032	1.57.....	0.737	1.70.....	0.745	1.83.....	0.099
1.32.....	0.001	1.45.....	0.063	1.58.....	0.741	1.71.....	0.748	1.84.....	0.020
1.33.....	0.002	1.46.....	0.087	1.59.....	0.746	1.72.....	0.733	1.85.....	0.014
1.34.....	0.003	1.47.....	0.131	1.60.....	0.745	1.73.....	0.661	1.86.....	0.012
1.35.....	0.004	1.48.....	0.178	1.61.....	0.739	1.74.....	0.622	1.87.....	0.009
1.36.....	0.004	1.49.....	0.261	1.62.....	0.737	1.75.....	0.594	1.88.....	0.008
1.37.....	0.005	1.50.....	0.396	1.63.....	0.737	1.76.....	0.598	1.89.....	0.006
1.38.....	0.006	1.51.....	0.594	1.64.....	0.737	1.77.....	0.634	1.90.....	0.004
1.39.....	0.007	1.52.....	0.653	1.65.....	0.737	1.78.....	0.665	1.91.....	0.002
1.40.....	0.008	1.53.....	0.693	1.66.....	0.721	1.79.....	0.673	1.92.....	0.000
1.41.....	0.012	1.54.....	0.721	1.67.....	0.709	1.80.....	0.665		
1.42.....	0.016	1.55.....	0.725	1.68.....	0.713	1.81.....	0.436		
1.43.....	0.024	1.56.....	0.729	1.69.....	0.729	1.82.....	0.218		

[4] See also http://www.ast.cam.ac.uk/instrumentation/irfilter/irfilter1.htm.

TABLE 10

TRANSMISSION OF K FILTER

λ	T	λ	T	λ	T	λ	T	λ	T
1.84.....	0.000	1.99.....	0.139	2.14.....	0.772	2.29.....	0.804	2.44.....	0.475
1.85.....	0.003	2.00.....	0.178	2.15.....	0.784	2.30.....	0.796	2.45.....	0.345
1.86.....	0.004	2.01.....	0.277	2.16.....	0.792	2.31.....	0.786	2.46.....	0.198
1.87.....	0.006	2.02.....	0.356	2.17.....	0.800	2.32.....	0.772	2.47.....	0.107
1.88.....	0.008	2.03.....	0.491	2.18.....	0.800	2.33.....	0.744	2.48.....	0.079
1.89.....	0.012	2.04.....	0.566	2.19.....	0.802	2.34.....	0.729	2.49.....	0.048
1.90.....	0.016	2.05.....	0.610	2.20.....	0.802	2.35.....	0.705	2.50.....	0.020
1.91.....	0.020	2.06.....	0.653	2.21.....	0.802	2.36.....	0.709	2.51.....	0.020
1.92.....	0.024	2.07.....	0.657	2.22.....	0.802	2.37.....	0.713	2.52.....	0.012
1.93.....	0.038	2.08.....	0.653	2.23.....	0.806	2.38.....	0.721	2.53.....	0.010
1.94.....	0.044	2.09.....	0.645	2.24.....	0.810	2.39.....	0.744	2.54.....	0.008
1.95.....	0.059	2.10.....	0.661	2.25.....	0.806	2.40.....	0.760	2.55.....	0.004
1.96.....	0.071	2.11.....	0.693	2.26.....	0.814	2.41.....	0.768	2.56.....	0.000
1.97.....	0.095	2.12.....	0.713	2.27.....	0.812	2.42.....	0.693		
1.98.....	0.115	2.13.....	0.748	2.28.....	0.810	2.43.....	0.554		

TABLE 11

TRANSMISSION OF K_s FILTER

λ	T	λ	T	λ	T	λ	T	λ	T
1.90.....	0.000	2.01.....	0.745	2.12.....	0.888	2.23.....	0.905	2.34.....	0.110
1.91.....	0.005	2.02.....	0.800	2.13.....	0.893	2.24.....	0.910	2.35.....	0.058
1.92.....	0.008	2.03.....	0.818	2.14.....	0.890	2.25.....	0.910	2.36.....	0.032
1.93.....	0.012	2.04.....	0.830	2.15.....	0.890	2.26.....	0.907	2.37.....	0.020
1.94.....	0.018	2.05.....	0.840	2.16.....	0.890	2.27.....	0.907	2.38.....	0.010
1.95.....	0.103	2.06.....	0.845	2.17.....	0.887	2.28.....	0.903	2.39.....	0.007
1.96.....	0.050	2.07.....	0.850	2.18.....	0.885	2.29.....	0.875	2.40.....	0.003
1.97.....	0.110	2.08.....	0.855	2.19.....	0.885	2.30.....	0.780	2.41.....	0.001
1.98.....	0.210	2.09.....	0.860	2.20.....	0.890	2.31.....	0.600	2.42.....	0.000
1.99.....	0.390	2.10.....	0.870	2.21.....	0.893	2.32.....	0.380		
2.00.....	0.600	2.11.....	0.880	2.22.....	0.900	2.33.....	0.210		

0.002 μm; H, 0.0025 μm; K or K_s, 0.003 μm. These shifts are are entirely negligible for the E82 standards or the new ones, all of which have approximately the same colors. As the shifts are less than 0.3% of the filter wavelengths, they are unlikely to be important even for the reddest stars.

REFERENCES

Barsony, M., Kenyon, S. J., Lada, E. A., & Teuben, P. J. 1997, ApJS, 112, 109
Burstein, D., & Heiles, C. 1982, AJ, 87, 1165
Campins, H., Rieke, G. H., & Lebofsky, M. J. 1985, AJ, 90, 896
Carter, B. S., & Meadows, V. S. 1995, MNRAS 276, 734
Casali, M., & Hawarden, T. 1992, JCMT-UKIRT Newsl., No. 4, 33
Greene, T. P., & Young, E. T. 1992, ApJ, 395, 516
Elias, J. H., Frogel, J. A., Hyland, A. R., & Jones, T. J. 1983, AJ, 88, 1027 (E83)
Elias, J. H., Frogel, J. A., Matthews, K., & Neugebauer, G. 1982, AJ, 87, 1029 (E82)
Hunt, L. K., Mannucci, F., Testi, L., Migliorini, S., Stanga, R. M., Baffa, C., Lisi, F., & Vanzi, L. 1998, AJ, 115, 2594
Jones, T. J., Hyland, A. R., Robinson, G., Smith, R., & Thomas, J. 1980, ApJ, 242, 132
Lasker, B. M., et al. 1988, ApJS, 68, 1
Luyten, W. J. 1979, LHS Catalogue (Minneapolis: Univ. Minnesota Press)
Murphy, D. C., Persson, S. E., Pahre, M. A., Sivaramakrishnan, A., & Djorgovski, S. G. 1995, PASP, 107, 1234
Persson, S. E., West, S. C., Carr, D. M., Sivaramakrishnan, A., & Murphy, D. C. 1992, PASP, 104, 204
Simons, D. 1996, Near Infrared Filter Bandpasses for Gemini Instruments (Cambridge: RGO)
Vural, K. 1994, in Infrared Astronomy with Arrays: The Next Generation, ed. I. S. McLean (Dordrecht: Kluwer), 355
Wainscoat, R. J., & Cowie, L. L. 1992, AJ, 103, 332
Young, A. T., Milone, E. F., & Stagg, C. R. 1994, A&AS, 105, 259